# Phase separation in dilute solutions of $^{3}$He in solid $^{4}$He

C. Huan, L. Yin, J. S. Xia, D. Candela, B. P. Cowan, and N. S. Sullivan

# Phase separation in dilute solutions of $^3$He in solid $^4$He

C. Huan[1], L. Yin[1], J. S. Xia[1], D. Candela[2], B. P. Cowan[3], and N. S. Sullivan[1*]

[1] *Department of Physics, University of Florida, Florida 32611, USA.*

[2] *Department of Physics, University of Massachusetts, Amherst, Massachusetts 01003, USA.*

[3] *Millikelvin Laboratory, Royal Holloway University of London, Egham, Surrey, TW20 OEX, UK.*

(Dated: February 21, 2017)

## Abstract

We report the results of studies of the phase separation of solid solutions of dilute concentrations of $^3$He in $^4$He. The temperatures and the kinetics of the phase separation were determined from NMR experiments for $^3$He concentrations $1.6 \times 10^{-5} < x_3 < 2.0 \times 10^{-3}$. The experimentally observed phase separation temperatures are found to be in excellent agreement with regular solution theory as augmented by Edwards and Balibar [Phys.Rev. B39,4083(1989)]. The growth of $^3$He droplets shows a $t^{\frac{1}{3}}$ time dependence at long times consistent with Ostwald ripening.

## I. INTRODUCTION

There is considerable interest in studying the phase separation of solid $^3$He–$^4$He mixtures as it represents a particularly clean example of the more general problem of phase separation in binary mixtures. In the case of solid helium mixtures one has high-purity defect-free crystalline samples, and these can be readily studied over a range of densities using high sensitivity techniques such as precision pressure measurements and NMR, or a combination of both.

The characteristic time scales are determined by volume diffusion in the solid and in the case of the solid heliums this is determined by quantum tunneling which is temperature-independent and much faster than diffusion in classical solids. As a result all stages of the dissolution and growth processes can be observed experimentally.[1] In this paper we compare the dynamics for the growth of precipitates from very dilute $^3$He samples with the observations at high $^3$He concentrations.

In addition to testing the regular solution theory for phase separation in solids, studies of $^3$He–$^4$He mixtures can investigate the kinetics of the growth of the different phases and in particular the late stage coarsening or Ostwald ripening[2,3] of the precipitated new phases.

## II. PHASE SEPARATION TEMPERATURES

In terms of regular solution theory the Helmholtz free energy of mixing is given by

$$F_m = Nx_3(1 - x_3)\Delta E + Nk_BT[x_3 \ln x_3 + (1 - x_3)\ln(1 - x_3)]. \tag{1}$$

Here $N$ is the total number of atoms, $x_3$ is the number concentration of $^3$He atoms and $\Delta E$ is the characteristic energy of the interaction, related to the critical temperature by $T_c = \Delta E/2k_B$. The first term is the regular solution energy of mixing and the second term contains the conventional entropy for a two state system. For temperatures below $T_c$ the Helmholtz free energy for given $x_3$ has two minima; these occur at $T = T_{ps}$:

$$T_{ps} = \frac{2(1 - 2x_3)}{\ln(x_3^{-1} - 1)}T_c. \tag{2}$$

For temperatures below $T_{ps}$ the homogeneous mixture is unstable and there is a transition into a $^3$He-rich and $^4$He-rich phase[4]. These transition points are also called binodals.

Between these minima there is a maximum in the free energy. The limit of stability, the spinodal, is determined by the point of inflexion for which $\partial^2 F_m/\partial x_3^2 = 0$; there will be two spinodals. Between the binodal and the spinodal the homogeneous mixture will be metastable, while between

the two spinodals the mixture will be unstable: Fig. 1. The metastable region can be relatively large, as indicated by the blue arrow in Fig. 1; at $T_{ps} = 0.7\,T_c$ it extends down to the spinodal at $0.31\,T_c$. The important point for the high-purity defect-free solid helium mixtures is that the absence of heterogeneous nucleation sites allows substantial supercooling to be achieved.
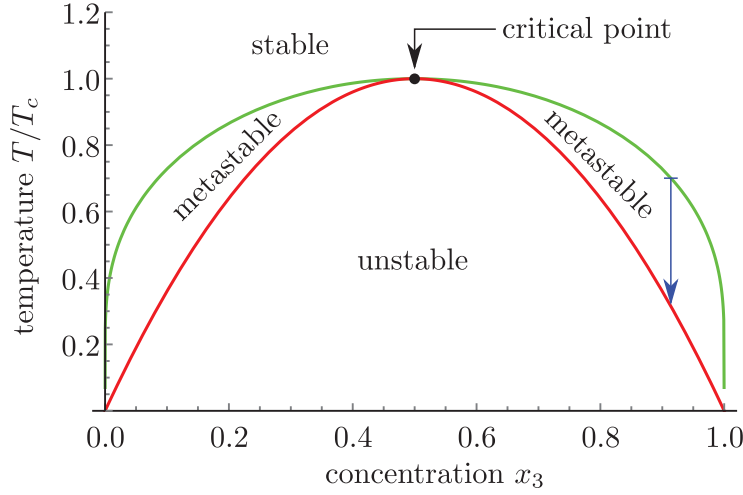


FIG. 1. The phase diagram for regular binary mixtures such as solid $^3$He–$^4$He mixtures. The green line is the binodal line; it designates the phase separation temperature, $T_{ps}$, and the red line is the spinodal line. The blue arrow shows a large amount of supercooling. (Color figure online).

The expression, from the theory of regular solutions, for the phase separation temperature of $^3$He–$^4$He solid mixtures as a function of concentration, Eq. (2), is in excellent agreement with the early measurements for concentrations $x_3 > 0.15$.[5] Deviations could occur from this symmetric solution due to the additional excess free energy associated with the large molar volume difference of $^3$He compared to $^4$He. This was considered by Mullin[6] and while there was some evidence for the consequent asymmetry in $T_{ps}$ versus $x_3$, in the work published by the group of Adams[7], careful measurements using x-ray scattering[8,9] showed that any excess free energy due to the molar volume difference of $^3$He and $^4$He was less than 1% of $\Delta E$.

More refined calculations of the phase diagram have been carried out by Edwards and Balibar[10](EB). Since, at the pressures considered, pure $^3$He forms a bcc lattice whereas pure $^4$He forms an hcp lattice, there must be a structural phase transition at some intermediate $x_3$. Thus EB considered the small difference in free energy due to the different crystal structures. They predicted a small asymmetry that should be observable at low values of $x_3$, together with a bcc/hcp coexistence

3

region. Recent experiments[11,12] confirm these calculations for $x_3$ concentrations down to 0.1%. Ganshin *et al.*[12] used the analysis of EB to calculate the correction

$$\Delta_3 = g_s^h(P,T) - g_3^b(P,T) \tag{3}$$

for the difference in the free energies of the metastable hcp and stable bcc phases of solid $^3$He labeled by the superscripts $h$ and $b$, respectively. One can write $\Delta_3 = \int_{P_3^0}^{P}(\delta V_3^0 + \beta P)dP$ where $\delta V_3^0 = V_3^h - V_3^b$ is the volume difference for the hcp and bcc phases, extrapolated to $T = 0$ K, and $\beta = 1.24 \times 10^{-3}$ cm$^3$/mole atmos. The value of $\delta V_3^0 = -0.09$ cm$^3$/mole at $P_3^0 = 102.9$ bar is taken from Straty and Adams[13]. For the pressure dependence found by Ganshin *et al.*[12] and Maidanov *et al.*[14] we find $\Delta_3 = 0.0135$ K at $P = 29$ bar. Using the interaction energy $\Delta E_h = 0.76$ K of EB we have for the phase separation temperature

$$T_{ps} = \frac{0.76(1 - 2x_3) + 0.0135}{\ln(x_3^{-1} - 1)}\text{ K.} \tag{4}$$

This prediction for the phase separation temperature for solid $^3$He and solid $^4$He precipitates as bcc and hcp crystallites, respectively, is shown by the solid green line in Fig. 2. The result is in excellent agreement with the experimental values reported by Ganshin *et al.*[12].

Recently there has been considerable interest in studying phase separation in low density solid $^3$He–$^4$He mixtures for which the $^3$He-rich phase after separation consists of liquid droplets.[1,18,19] One of the main interests in studying the phase separation of $^3$He–$^4$He solid mixtures is to explore the kinetics of the phase transition which is a fundamental problem in condensed matter physics. The phase transitions can be accurately determined from measurements of the NMR amplitudes.[15,20] Because of the small nuclear spin susceptibility of the degenerate Fermi liquid in the nearly pure $^3$He droplets, one observes a sharp drop in the NMR amplitudes at the phase transition. This change in the NMR amplitudes is illustrated for several $x_3$ concentrations in Fig. 3. Careful measurement of the NMR amplitudes above the phase transitions is also very important for *in situ* determinations of a sample's true $^3$He concentration. This technique was shown to be critical for studies of very dilute samples of $^3$He in $^4$He because of the appreciable loss of $^3$He in a prepared sample gas mixture due to plating on the walls of the capillary filling tubes at low temperatures as the sample is condensed into an experimental cell.[21] The novel features of these studies is that high sensitivity NMR techniques were used to obtain accurate results for the growth of the $^3$He nanodroplets for very dilute $^3$He samples (down to 16 ppm). This accuracy was achieved by employing a low temperature RF amplifier operating at dilution refrigerator temperatures and located close to the NMR sample cell.[22]
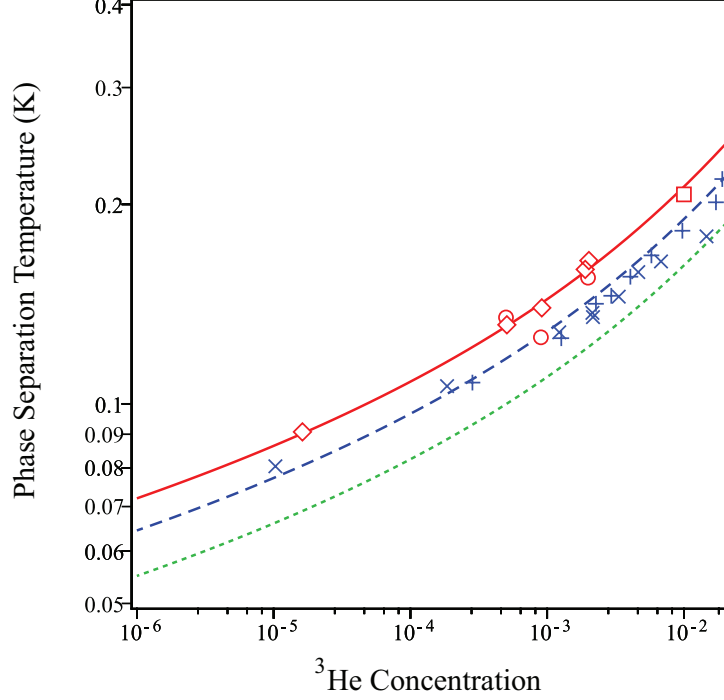
4

FIG. 2. Variation of the phase separation temperatures for dilute solutions of $^3$He in solid $^4$He. Solid red line, $\Delta_3 = 0.255$ K (Eq. 8), $^3$He precipitate liquid droplets; dashed blue line, $\Delta_3 = 0.0135$ K (Eq. 4), precipitates all solid; dotted green line, $\Delta_3 = 0$; blue crosses, Ganshin *et al.* – cooling[12]; rotated blue crosses, Ganshin *et al.* – warming[12]; red diamonds, Huan *et al.* – NMR amplitude[15]; red circles, Huan *et al.* – NMR relaxation[15]; red square, Kingsley *et al.*[16]. (After Fig. 17 of Ref.[17]). (Color figure online).

There is an additional shift in the phase separation curve when the $^3$He precipitate is a liquid. For the $^3$He-rich phase one treats the rare $^4$He particles as a gas, and the chemical potential is given by EB, $\mu_4(P, T, x_3) = g_4^L(P) + E_4 + k_B T \ln[(\frac{T^*}{T})^{3/2}(1 - x_3)]$ where $E_4$ is the chemical potential for one atom of $^4$He in the $^3$He droplet at $T = 0$ and $T^*$ is a parameter for the dilute gas of quasiparticles: EB, and Pettersen *et al.*[23]. Using the values reported by Laheurte[24] we find $E_4 = 0.45 \pm 0.005$ K on extrapolating to $P = 29$ bar. The last term in the expression for $\mu_4(P, T, x_3)$ is difficult to estimate accurately. Using the tables in Edwards and Pettersen one finds $T \ln[(\frac{T^*}{T})^{3/2}(1 - x_3)] \approx -0.18$ K at $T \sim 0.15$ K.

Following EB the free energy $g_4^L(P)$ can be calculated with respect to the melting curve at $P_4^m$ of $^4$He with

$$g_4^L = g_4^h + \int_{P_4^m}^{P} (v_4^L - v_4^h) dP \tag{5}$$

$v_4^L - v_4^h = 2.165[1 - (P - P_4^m)/83] = 2.06$ cm$^3$/mole. Hence $g_4^L - g_4^h = 0.095$ K. The $^3$He
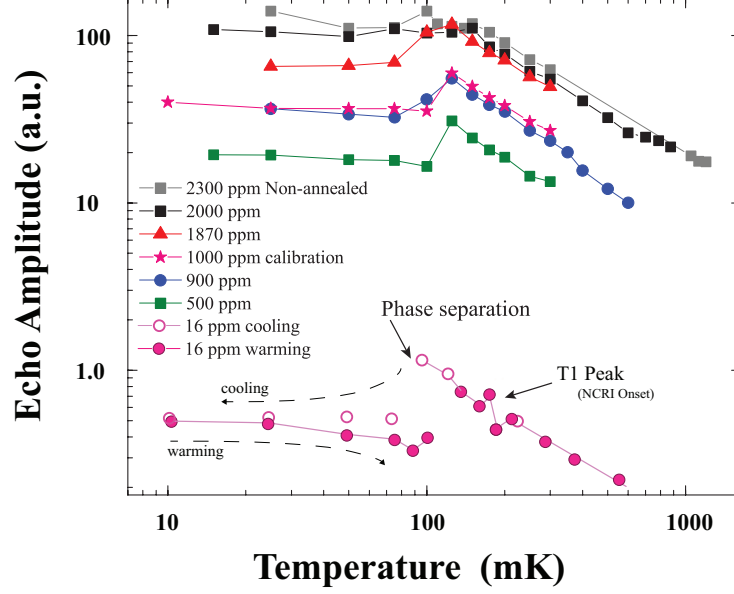
FIG. 3. Change in NMR amplitudes of $^3$He NMR signal occuing at the phase separation in low density solid $^3$He–$^4$He mixtures. (Reproduced with permission from Fig. 2 of Candela *et al.*[20]). (Color figure online).

chemical potential in the liquid phase is found from

$$g_3^L = g_3^b + \int_{P_4^m}^{P} (v_3^L - v_3^h)dP. \tag{6}$$

From the data given by EB we find $g_3^L - g_3^b = 0.058$ K. For the phase separation temperature for the formation of $^3$He-rich droplets we therefore find

$$T_{ps}^{L(calc)} = \frac{0.76(1 - 2x_3) + 0.31}{\ln[x_3^{-1} - 1]} \, \text{K}. \tag{7}$$

The best fit to the experimental data is shown by the solid red curve of Fig. 2 given by

$$T_{ps}^{L(expt)} = \frac{0.76(1 - 2x_3) + 0.255}{\ln[x_3^{-1} - 1]} \, \text{K}. \tag{8}$$

## A.   Kinetics of Phase-Separation of $^3$He–$^4$He solid mixtures.

Understanding the kinetics of phase separations is a fundamental problem of considerable importance in condensed matter physics because of the role it plays in the preparation of new materials where the rate processes need to be understood to produce high quality high strength alloys and to fully describe the phase transitions undergone by polymers[25]. The transition is first order,

with a conserved order parameter. One open question for this class of systems is whether there is a well-defined universality class that describes the critical fluctuations. (Of course, away from the critical concentration the fluctuations diverge at the spinodal, not at the binodal.)

As one enters the temperature region where it is favorable to have separate phases the system becomes metastable and small nuclei of the separate phases form as the result of fluctuations that can overcome the energy barrier separating the two phases. If some of these nuclei exceed a critical size they can grow into stable clusters. The advantage of studying $^{3}$He–$^{4}$He mixtures is that the system can be prepared in a state of high purity with only extremely small concentrations of impurities or defects. One can then realize relatively large supercooling because of the wide separation of the phase separation temperature and the spinodal temperature, together with the rarity of nucleation sites. In addition, the time scales are experimentally accessible (order of hours) for the solid helium mixture because of the high diffusion rate of $^{3}$He in the mixture. Considerably larger time scales occur for other systems, especially metallic alloys.

The growth of the seed nuclei in a uniform supersaturated mixture is known as homogeneous nucleation and was first successfully observed by Penzev *et al.*[19]. After the period of homogeneous nucleation the remaining phase is largely depleted of $^{3}$He (if we are considering the nucleation of $^{3}$He clusters) and one then observes a different and much slower evolution known as Ostwald ripening[2,3] or coarsening of the $^{3}$He droplets as the sub-critical droplets dissolve and the remote $^{3}$He atoms diffuse to and are captured by the larger droplets. The existence of all three stages of the phase separation process in the same $^{3}$He–$^{4}$He mixture system has been observed by Poole *et al.*,[1,26] using a combination of NMR techniques and pressure measurements.

The characteristics of the homogeneous growth before Ostwald ripening are determined from considerations of the continuity equation relating the distribution function, $f(n,t)$, for the number of elements $n$ in a growing cluster, and the flux, $I_n(t)$, toward the cluster.[27] The continuity equation is given by

$$\frac{\partial f}{\partial t} = -\frac{\partial I_n}{\partial n}.$$ (9)

If $x(t)$ is the concentration of atoms in the new phase at time $t$ and $x_0$ is the initial concentration, then

$$x_0 = x(t) + \int_0^\infty f(n,t)n\,dn$$ (10)

$f(n,t)|_{n\to 0} \to x(t)$ and $f(n,t)|_{n>1,t=0} = 0$. The flux in size space for a cluster of size $n$ is given

by

$$I_n = -W_{n,n+1} \left[ \frac{\partial f}{\partial n} + \frac{\delta}{\delta n} \frac{\Delta \Phi}{k_B T} \right] \tag{11}$$

$W_{n,n+1}$ is the probability of absorbing one atom in time $t$ and is related to the usual diffusion constant $D$ by $W = \alpha x n^{2/3} D/a^2$ with $\alpha$ a geometrical factor of order unity, and $a_0$ is the lattice spacing in the original matrix. The change in thermodynamic potential $\Delta \Phi(n)$ is given by

$$\Delta \Phi(n) = n(\mu^N - \mu^O) + 4\pi a^2 \sigma n^{2/3} \tag{12}$$

where $\mu^N$ and $\mu^O$ are the chemical potentials for the new cluster and the original solution, respectively. $\sigma$ is the surface tension. We have

$$\frac{\Delta \Phi}{k_b T} = -n \ln \frac{x}{x_\infty} + \frac{4\pi \sigma a^2}{k_B T} n^{2/3} \tag{13}$$

which can be written as

$$\frac{\Delta \Phi}{k_b T} = \frac{\beta}{2} n^{2/3} - n\beta(n_c^{-1/3} - n^{-1/3}) \tag{14}$$

with $\beta = (8\pi \sigma a^2)/(3k_b T)$. The critical size, $n_c$, of the new droplet is then given by $\delta \Delta \Phi/\delta n = 0$, or

$$n_c^{1/3} = \beta[\ln(x_0/x_\infty)^{-1}]; \tag{15}$$

$x_0$ and $x_\infty$ are the initial and final concentrations, respectively.

The important factor determining the kinetics is the flux at $n = n_c$ given by

$$I_0 = \left( \frac{3\beta}{2\pi} \right)^{1/2} x_0^2 \exp \left[ -\frac{\Delta \Phi}{k_B T} \right] = \left( \frac{3\beta}{2\pi} \right)^{1/2} x_0^2 \exp \left[ -\frac{\beta^3}{2(\ln 2[c_0/c_\infty])^2} \right]. \tag{16}$$

Because of the exponential dependence of $I_0$ on concentration, the clusters grow extremely rapidly and nucleation is seen only for a very small supersaturation. At the end of the nucleation the clusters are characterized by a maximum concentration per lattice site. Slezov and Schmelzer[27] find this to be given by

$$N_M = (4x_0)^{1/4} \left( \frac{I_0}{\beta} \right)^{3/4}. \tag{17}$$

Smith *et al.*[18] find $N_M \approx 10^{-15}$ at $x \approx 1\%$, and this is in good agreement with their measurements of the NMR amplitudes. For the studies of Huan *et al.*[15] for $x \approx 0.1\%$, we expect $N_M \approx 10^{-14}$.

The characteristic time scale for this homogeneous nucleation is given by

$$\tau_N = \frac{a_0^2}{3D} x_0^{-1/3} N_M^{2/3}. \tag{18}$$

8

This expression yields time constants for homogeneous nucleation of the order of an hour. In Fig. 4 we show the growth observed by Huan *et al.*[15] following a drop in temperature of $100$ mK into the metastable region of the phase diagram. Following a delay of about $1.1$ h (attributed to nucleation) they observe a growth that is approximately exponential with a time constant of $2.4 \pm 0.3$ h (solid red line of Fig. 4). The best fit to the data, however, requires a small additional very slow growth shown by the difference between the solid red and dashed blue curves of Fig. 4 . This slow growth after the homogeneous nucleation period is attributed to the Ostwald ripening.

Following Slezov and Schmelzer,[27] the Ostwald ripening follows a $t^{1/3}$ dependence. Poole and Cowan[26] note that this dependence can be understood in terms of a simple scaling argument. For a droplet of radius $r(t)$ the curvature varies as $r(t)^{-1}$ and the concentration gradients vary as $\sigma/r(t)^2$. The diffusive flux is therefore of the order of $D\sigma/r(t)^2$, and the growth rate is given by

$$\frac{dr(t)}{dt} \sim \frac{D\sigma}{r(t)^2} \tag{19}$$

which has a solution $r(t) \sim (\sigma D t)^{1/3}$. Following a detailed numerical analysis, Slezov and Schmelzer[27] find

$$r(t) = V_M^{1/3}(t/t_{Ost})^{1/3} \tag{20}$$

where $V_M$ is the volume per atom and the characteristic time scale for the ripening is $t_{Ost} = \frac{4}{9}x_\infty \sigma D/(k_B T)$. $t_{Ost}$ is typically $3 - 5$ h. for concentrations in the range $0.1 - 1.0$ %.

In order to highlight the behavior at long times we plot in Fig. 5 the excess growth at long times compared to the exponential growth of Fig. 4. The solid red line is a fit to the ripening stage which varies as $(t/t_{Ost})^{1/3}$ with $t_{Ost} = 4.05$ h. The fit is reasonably good given the approximations that have been made.

III. **CONCLUSION**

The analysis of recent experimental results for the phase separation of solid $^3$He-$^4$He mixtures, dilute in $^3$He, show that the observed phase separation temperatures are in excellent agreement with theory of Edwards and Balibar[10] provided one includes the difference in free energy between the liquid and solid states and also accounts for the pressure difference of the experiments which also changes the free energy. The observed growth of liquid $^3$He droplets for very dilute $^3$He concentrations (down to 16 ppm) show an Ostwald ripening behavior at long times in agreement with the predicted power law dependence of $t^{1/3}$.
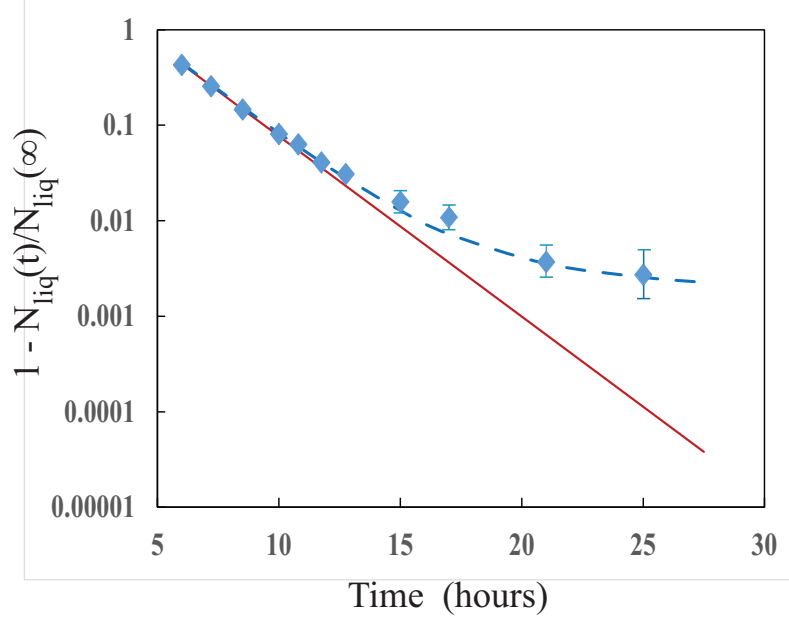
FIG. 4. Observed decay of the NMR amplitude following the formation of droplets after a 100 mK temperature change at the phase separation temperature. Diamonds, Huan *et al.*[15], solid line exponential decay with time constant 2.20 hours, and the broken line represents an added $t^{1/3}$ dependence to fit the data at long times. (Color figure online).
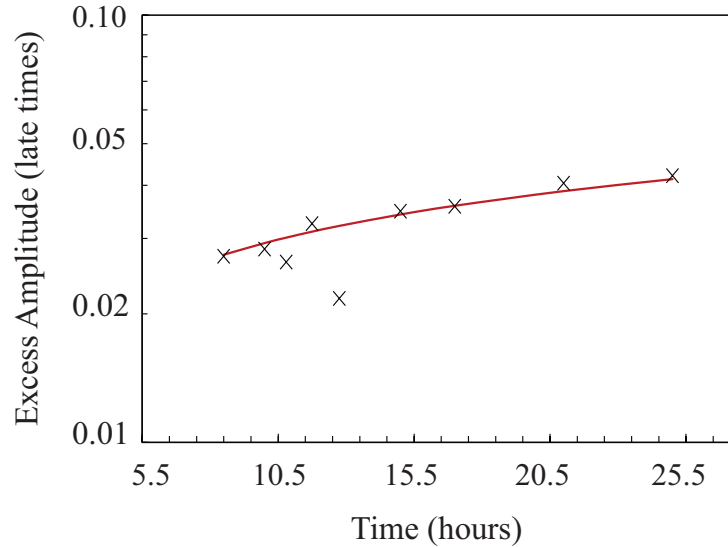


FIG. 5. Comparison of the excess amplitude at late times for droplet growth of $^3$He during phase separation (shown in Fig. 4) relative to a pure exponential decay. The solid line is the fit for a $t^{1/3}$ dependence. (Color figure online).

## IV. ACKNOWLEDGEMENTS

## REFERENCES

\* sullivan@phys.ufl.edu

[1] M. Poole, J. Saunders, and B. Cowan, Phys. Rev. Lett. **100**, 075301 (2008).

[2] W. Ostwald, Zeit. für Phys. Chemie **22**, 289 (1897).

[3] I. M. Lifshitz and V. V. Slyozov, J. Phys. Chem. Solids **19**, 35 (1961).

[4] B. Cowan, *Topics in Statistical Mechanics* (Imperial College Presss, 2005).

[5] D. O. Edwards., A. S. McWilliams, and J. G. Daunt, Phys. Rev. Lett. **9**, 195 (1962).

[6] W. J. Mullin, Phys. Rev. Lett. **20**, 254 (1968).

[7] M. F. Panczyk, R. A. Scribner, J. R. Gonano, and E. D. Adams, Phys. Rev. Lett. **21**, 594 (1968).

[8] B. A. Fraass and R. O. Simmons, Phys. Rev. B **36**, 97 (1987).

[9] S. W. Ehrlich and R. O. Simmons, J. Low Temp. Phys. **68**, 125 (1987).

[10] D. O. Edwards and S. Balibar, Phys. Rev. B **39**, 4083 (1989).

[11] V. A. Shvarts, N. P. Mikhin, E. Y. Rudavskii, Y. A. Tokar', A. M. Usenko, and V. A. Mikheev, Low Temp. Physics **20**, 505 (1994).

[12] A. N. Gan'shin, V. N. Grigor'ev, V. A. Maidanov, N. F. Omelsenko, and A. A. Penzev, Low Temp. Phys. **26**, 869 (2000).

[13] G. C. Straty and E. D. Adams, Phys. Rev. **150**, 123 (1966).

[14] V. Maidanov, A. Ganshin, V. Grigorev, A. Penzev, E. Rudavskii, and A. Rybalko, J. Low Temp. Phys. **122**, 475 (2001).

[15] C. Huan, S. Kim, L. Yin, J. Xia, D. Candela,  and N. Sullivan, J. Low Temp. Phys. **162**, 167 (2011).

[16] S. Kingsley, V. Maidanov, J. Saunders,  and B. Cowan, J. Low Temp. Phys. **113**, 1017 (1998).

[17] N. S. Sullivan, Prog. Nucl. Mag. Reson. Spectr. **90  91**, 74  (2015).

[18] A. Smith, V. A. Maidanov, E. Y. Rudavskii, V. N. Grigor'ev, V. V. Slezov, M. Poole, J. Saunders,  and B. Cowan, Phys. Rev. B **67**, 245314 (2003).

[19] A. Penzev, A. Ganshin, V. Grigor'ev, V. Maidanov, E. Rudavskii, A. Rybalko, V. Slezov,  and Y. Syrnikov, J. Low Temp. Phys. **126**, 151 (2002).

[20] D. Candela, C. Huan, S. S. Kim, L. Yin, J. S. Xia,  and N. S. Sullivan, J. of Phys.: Conf. Series **568**, 012017 (2014).

[21] S. S. Kim, C. Huan, L. Yin, J. Xia, D. Candela,  and N. S. Sullivan, Phys. Rev. Lett. **106**, 185303 (2011).

[22] C. Huan, S. Kim, L. Phelps, J. Xia, D. Candela,  and N. Sullivan, J. Low Temp. Phys. **158**, 692 (2010).

[23] M. Pettersen, D. O. Edwards,  and T. G. Culman, J. Low Temp. Phys. **89**, 473 (1992).

[24] J. P. Laheurte, J. Low Temp. Phys. **12**, 127 (1973).

[25] J. T. Cabral, J. S. Higgins, N. A. Yerina,  and S. N. Magonov, Macromolecules **35**, 1941 (2002).

[26] M. Poole and B. Cowan, J. Low Temp. Phys. **134**, 211 (2004).

[27] V. V. Slezov and J. Schmelzer, Physics of the Solid State **39**, 1971 (1997).